



Trans. Nonferrous Met. Soc. China 33(2023) 3712-3724

Transactions of Nonferrous Metals Society of China

www.tnmsc.cn



Effect of reducing heat input on autogenous TIG welding of Ti-6Al-4V alloy

Kamlesh KUMAR, Manoj MASANTA

Department of Mechanical Engineering, National Institute of Technology Rourkela, Rourkela 769008, India

Received 23 May 2022; accepted 17 August 2022

Abstract: 3 mm-thick Ti-6Al-4V alloy plates were welded in butt joint configuration through autogenous TIG welding method using a trailing gas shielding arrangement. After attaining full penetrated weld joint with appropriate heat input, subsequent experiments were conducted by reducing the heat input, which was obtained through combination of higher welding current and scan speed. An in-depth microstructural analysis of the weld joint executed under different heat input conditions shows a strong correlation with the microhardness, tensile strength, and flexural strength of the weld joint. A significant improvement in the mechanical properties of the weld joint was perceived for employing lower heat input. Alteration in the primary-α, primary-β, and martensite-α phases, due to the variation in heat input, amended the mechanical properties of the weld joint under lower heat input condition. With the reduction of heat input from 0.406 to 0.232 kJ/mm, the tensile and flexural strengths of the weld joint increased from 1020 to 1070 MPa, and from 1015 to 1950 MPa, respectively. The tensile strength of the joint reached up to 98% of the base material at minimum heat input (0.232 kJ/mm). The experimental results show the potential of TIG welding for joining Ti-6Al-4V alloy under low heat input condition.

Key words: TIG welding; Ti-6Al-4V alloy; heat input; tensile strength; microstructure

1 Introduction

Ti-6Al-4V alloy encounters a wide range of industrial applications due to its high specific strength, low density, and excellent corrosion resistance [1,2]. It needs an enduring joining method that enables to provide an excellent joint efficiency with minimum energy expenses. AKMAN et al [3] and WANG and WU [4] showed that Ti-6Al-4V alloy is usually welded by the advanced welding methods like laser beam welding (LBW) and electron beam welding (EBW), which exhibits outstanding mechanical characteristics without obviously affecting the bulk characteristic of the material. Nevertheless, high equipment cost, technological complexities, and difficulties in controlling the welding conditions are the crucial

concerns associated with these welding processes. PANDEY et al [5] showed that simplicity, cost-effectiveness, and potential to produce good quality joint endorse the TIG welding as an effective and efficient joining method for a wide range of materials.

CAO and JAHAZI [6] showed that titanium and its alloys have an affinity towards the reaction with atmospheric gases at elevated temperatures, which augmented its welding complexity during fusion welding methods. According to LEYENS and PETERS [7], above 450 °C, by absorbing oxygen, nitrogen, and hydrogen from the atmosphere, Ti-based alloy produces brittle phases that reduce the welding strength substantially. Hence, shielding of weld melt pool during and after the welding becomes indispensable for titanium alloy joining. In this regard, LISIECKI [8] proposed

a multi-nozzle shielding system to protect the weld melt pool during the laser welding of Ti-6Al-4V alloy. In separate work, KARPAGARAJ et al [9] recommended a trailing shielding arrangement, which locally shielded the weld melt pool during and after the TIG arc scanning.

Further, KUMAR and SHAHI [10] recognized current and scan speed as the most significant parameters that define the energy density employed during the TIG welding. It was also reported that the scan speed led to the shape of the molten pool, and the welding current influenced the size of the weld bead [11]. KARPAGARAJ et al [9] showed that suitable welding current and scan speed combination produced appropriate bead geometry, which exhibited weld strength superior to the strength of commercial pure (CP) titanium.

A recent study by LIU et al [12] has revealed that minimum heat input obtained through combination of a high current and high scan speed is favorable for the economical production of a defect-free weld joint. It was reported that the weld bead geometry, microstructure, and mechanical properties of the TIG-welded joints are strongly dependent on the heat input, which is controlled by the combination of welding current, scan speed, and arc voltage [13]. KUMAR and SHAHI [10] showed that due to the formation of smaller dendrite and smaller inter-dendritic spacing in the fusion zone, the weld joint obtained at low heat input possessed better mechanical properties than those obtained at higher heat input. It was also suggested that higher welding current and lower speed combination exhibited better weld quality in terms of penetration depth and tensile strength [9]. BOCCARUSSO et al [14] reported that for reducing the specific heat input, the weld bead width reduced expressively compared to the penetration depth, which resulted in a higher weld aspect ratio and eventually higher welding strength.

Although the effects of welding parameters, i.e., processing current (for TIG welding), beam power (for LBW), and scan speed were studied on the weld joint quality for various advanced materials, in very limited works, similar analysis was conducted for Ti-6Al-4V alloy. In the present work, 3 mm-thick Ti-6Al-4V alloy plates were TIG-welded in butt joint configuration with the support of a trailing shielding gas arrangement. The weld bead geometry, macro-, and micro-structures

of the fusion zone (FZ) and heat-affected zone (HAZ) for the welding current variation were evaluated. An appropriate welding current for full penetration welding was identified. After obtaining a full penetration welding with adequate strength, additional experiments were performed by reducing the heat input, which was attained by increasing the welding current and scan speed simultaneously. Detailed microstructural analysis and assessment of mechanical performance, i.e., microhardness, tensile strength, and flexural strength of the weld joint, were carried out, and the effect of heat input was evaluated.

2 Experimental

For the present investigation, 3 mm-thick Ti-6Al-4V plates with dimensions 50 mm \times 75 mm were used as work-piece. The faying surfaces of the plates were cleaned by polishing them with abrasive paper and acetone to remove any pre-existing oxide layer and other contaminations. A TIG welding machine (Fronius MV 2200) equipped with a semiautomated moving unit was used to perform the single-pass autogenous butt joint. To protect the weld melt pool during and after the TIG arc scanning, argon gas was supplied through a secondary trailing shielding nozzle and a fixed bottom shielding arrangement with a flow rate of 20 L/min as illustrated in Fig. 1. A 2.4 mm diameter tungsten electrode was used, and 3 mm gap between the workpiece and the electrode tip was maintained for the entire set of experiments. The appropriate measure was taken for the alignment of the plates to attain uniform welding. Before actual experiments, trial experiments of butt welding were carried out by varying the welding current and scan speed, and a suitable heat input condition for full penetration welding was identified. Based on the results, experiments were performed by increasing the welding speed and current simultaneously, so that the employed heat input followed a reducing trend. The detailed experimental conditions are presented in Table 1. A standard heat input equation $(H=\eta VI/s, H \text{ is heat input per unit length, and } V, I, s,$ and η are voltage, current, scan speed, and TIG welding efficiency, respectively) for TIG welding, which was reported by MRIDHA and RAKER [15] and many other research groups, was considered to assess the heat input. As suggested by various

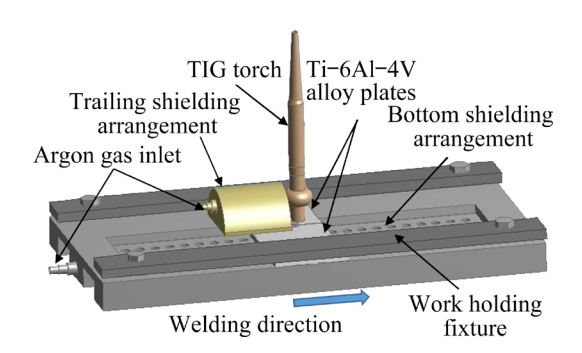


Fig. 1 Schematic diagram of TIG welding setup with trailing secondary shielding and bottom shielding arrangement

Table 1 TIG welding conditions at different heat inputs

No.	Current/A	Speed/ $(mm \cdot s^{-1})$	Average voltage/V	Heat input/ (kJ·mm ⁻¹)
1	150	2.3	13	0.406
2	175	3.5	13	0.312
3	200	4.7	13	0.265
4	220	5.9	13	0.232

researchers [15,16], the TIG welding efficiency for the present investigation was considered to be 48%.

After performing the welding, the samples of specific dimensions were sectioned from the welded plates. The specimens were then polished through the standard metallographic procedure and etched with Kroll's reagent (HF: 3 mL, HNO₃: 2 mL, and distilled water: 95 mL) to expose the weld bead and its microstructure. The weld bead dimensions and morphology of the FZ, HAZ, and unaffected base material (BM) were identified from the optical microscopy images and analyzed through Image analysis software. Besides, the microhardness across the weld bead (at 0.5 mm depth from the top surface) covering the FZ, HAZ, and unaffected BM was measured using a Vickers microhardness tester with 200 g load and 10 s indentation time. The hardness value was measured along the entire weld bead by maintaining 0.5 mm spacing between the successive indentations.

For the assessment of tensile strength, the specimens were cut from the welded plates as per ASTM E—8 standard, according to the dimensions illustrated in Fig. 2. The transverse tensile strength for the welded samples and the base material was measured at room temperature, using a computer-controlled universal testing machine with a cross-head speed (strain rate) of 0.5 mm/min. The

fractured surfaces of the tensile specimens were analyzed through a scanning electron microscope. The flexural strength of the weld joint was measured through a three-point bend test setup attached to the same universal testing machine. The bend test specimens (150 mm × 20 mm × 3 mm) were prepared as per IS:1599—1985 standard, and the bend test was performed with a cross-head speed of 0.5 mm/min, by keeping the weld-face under tension and weld-root under compression. The schematic representation of the bend test arrangement is shown in Fig. 3. The test was continued till 30 mm downward displacement of the bending punch or the failure of the test specimen, whichever is earlier.

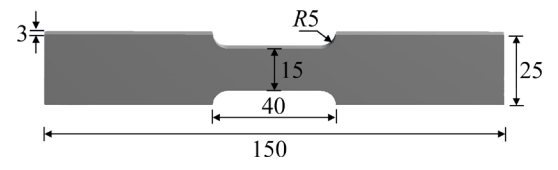


Fig. 2 Schematic diagram of tensile test specimen as per ASTM E—8 standard (Unit: mm)

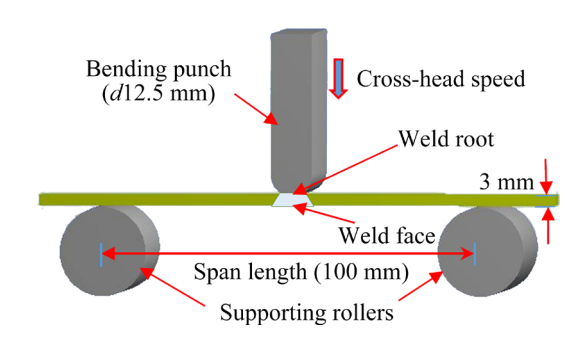


Fig. 3 Schematic representation of bend test arrangement

3 Results and discussion

From the analysis of the trial experiment, it was revealed that for 150 A current and 2.3 mm/s scan speed, a full penetration welding with adequate strength was achieved. The heat input per unit length under this condition was calculated to be 0.406 kJ/mm. Further, the experiment of KUMAR and SHAHI [10] showed that relatively low heat input by maintaining a higher welding current enhanced the quality of the welding by improving its strength. Accordingly, experiments were performed by reducing the heat input, which was obtained by increasing the welding current and speed simultaneously, as shown in detail in the experimental procedure.

3.1 Weld bead geometry

The cross-sectional images of the weld joints under different heat input conditions are illustrated in Fig. 4(a), from which the weld penetration depth, FZ, HAZ, and unaffected BM were identified. The images revealed the formation of full penetrated (3 mm) welding under all different heat input conditions, except for 0.312 kJ/mm. The weld melt pool width, HAZ width, and the weld aspect ratio were plotted against the employed heat input and depicted in Figs. 4(b-d), respectively. It was evident that the weld melt pool width and HAZ width were increased almost steadily with the increase of heat input; whereas, the weld aspect ratio was reduced gradually.

In the present experiments, lower heat input was obtained with a high current and high scan speed combination. It was reported that with the increase of welding current, the arc force increased gradually, which enhanced the weld penetration depth more prominently as compared to the melt pool width [17]. Furthermore, the increase in scan speed narrowed down the weld melt pool width, and with the increase in welding current, the melting depth increased considerably [11].

Henceforth, it is expected that with the reduction of heat input (by increasing scan speed and welding current simultaneously), the weld bead width will also decrease. In the present case, after considering a full penetration welding (3 mm), with the reduction of heat input, the weld aspect ratio increased due to the reduction of melt pool width. The reduction of heat input by increasing the welding speed further caused lower arc-metal interaction and consequently reduced the melt pool width. A similar observation was also reported by BOCCARUSSO et al [14] for laser welding of 3 mm-thick Ti-6Al-4V alloy.

3.2 Microstructure

Figures 5(a, b) depict the microstructures of the unaffected BM interface and the FZ of the welded joint produced at 0.406 kJ/mm heat input (marked 1 and 2 in Fig. 4(a)), respectively. The images show that the unaffected BM consists of the equiaxed α phase (white shaded) and intergranular β phase (dark shaded), distributed along the boundaries of α phases; whereas, the HAZ consists of primary- α , primary- β , and acicular- α phases. On the contrary, the FZ (Fig. 5(b)) was characterized by relatively

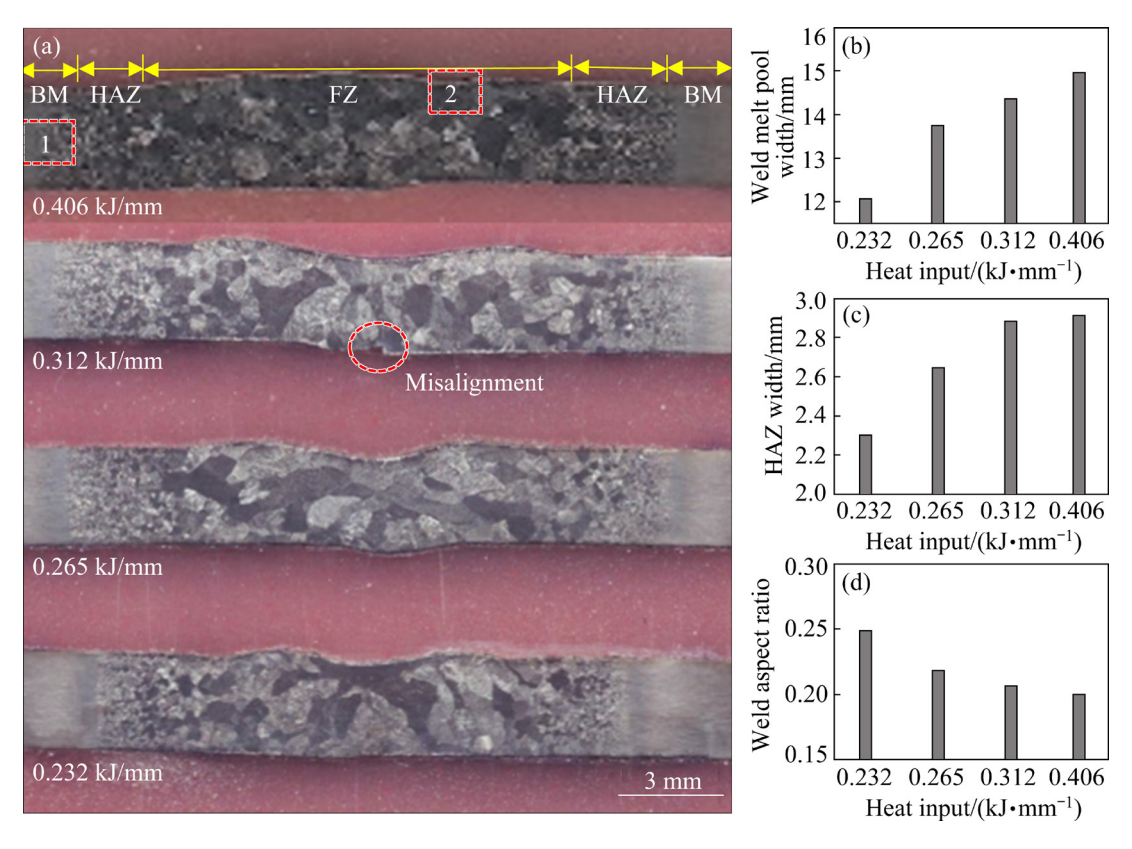


Fig. 4 Cross-section morphologies of weld bead under different heat inputs (a), and effect of heat input on weld melt pool width (b), HAZ width (c) and weld aspect ratio (d) for TIG-welded Ti-6Al-4V alloy

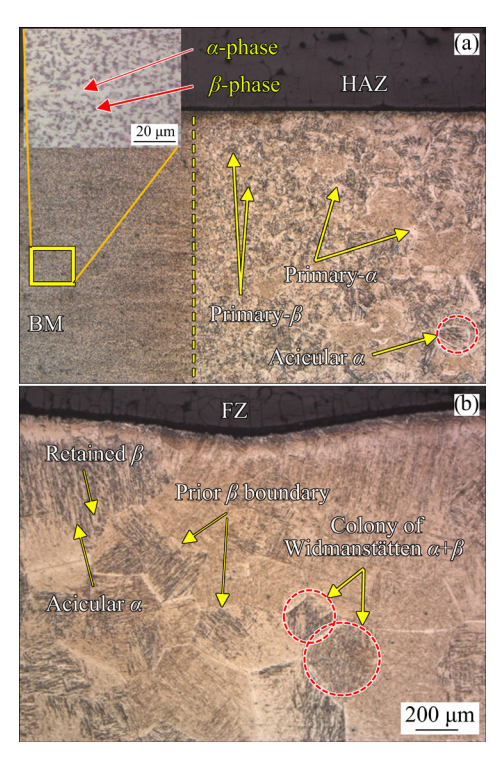


Fig. 5 Microstructures of BM (inset) and HAZ (a), and FZ (b) of weld joint at heat input of $0.406~\mathrm{kJ/mm}$

large size grains consisting of Widmanstätten α colony separated by prior β boundaries.

According to the research results in Ref. [6],

the morphology appeared in the HAZ corresponds to the structure of Ti-6Al-4V alloy obtained due to quenching occurring below β -transus temperature (about 985 °C). Further, the evolved microstructure in the FZ was mainly obtained due to the diffusional transformation of β to acicular- α at or above β -transus temperature during the solidification of the molten Ti-6Al-4V alloy [18]. DING et al [19] showed that during TIG welding of Ti-6Al-4V alloy, unlike the FZ, in the HAZ, α and β phases were not transformed completely to hightemperature β phase. It was also reported that the initial α phase and a fraction of β phase remained unaffected below the β -transus temperature. During solidification, rapid cooling allowed a small portion of β phase to transform into martensitic α phase. Hence, a mixed mode of transformation occurred, and a mixed type structure was obtained in the HAZ.

3.3 Grain size

From the magnified images of the weldment under different heat input conditions, as shown in Fig. 6, the individual grain size was measured using image analysis software. The grain size distribution in the FZ under different heat input conditions is illustrated in Fig. 7. The plots show an almost normal

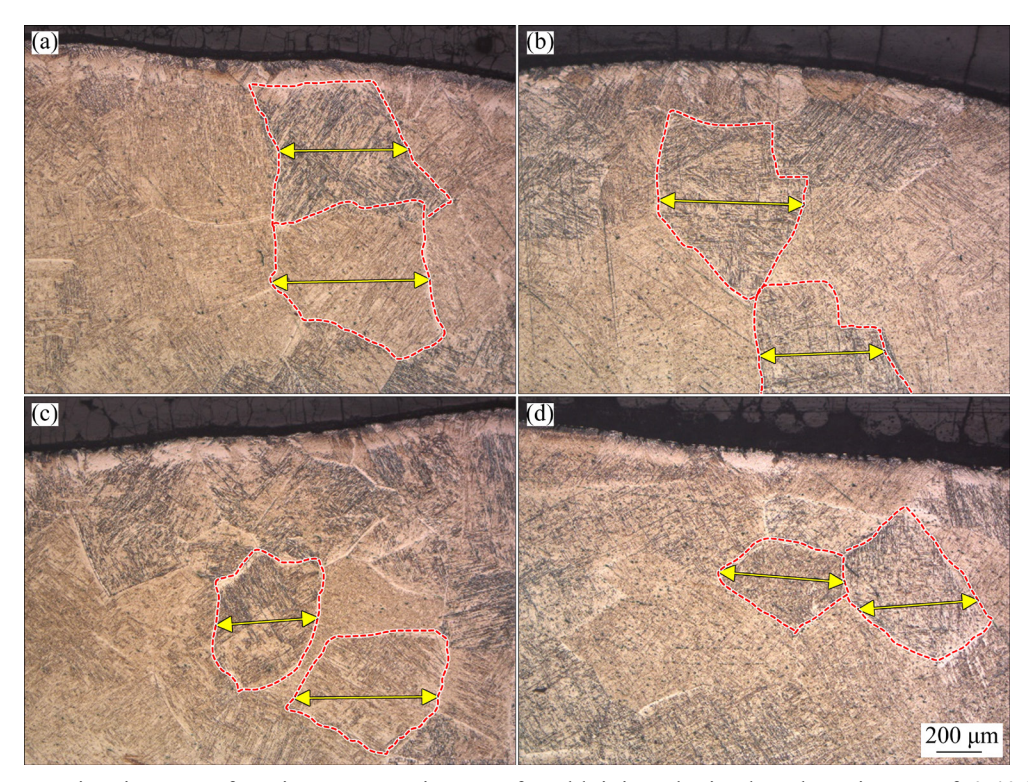


Fig. 6 Representative images of grain structure in FZ of weld joint obtained at heat inputs of 0.406 kJ/mm (a), 0.312 kJ/mm (b), 0.265 kJ/mm (c), and 0.232 kJ/mm (d)

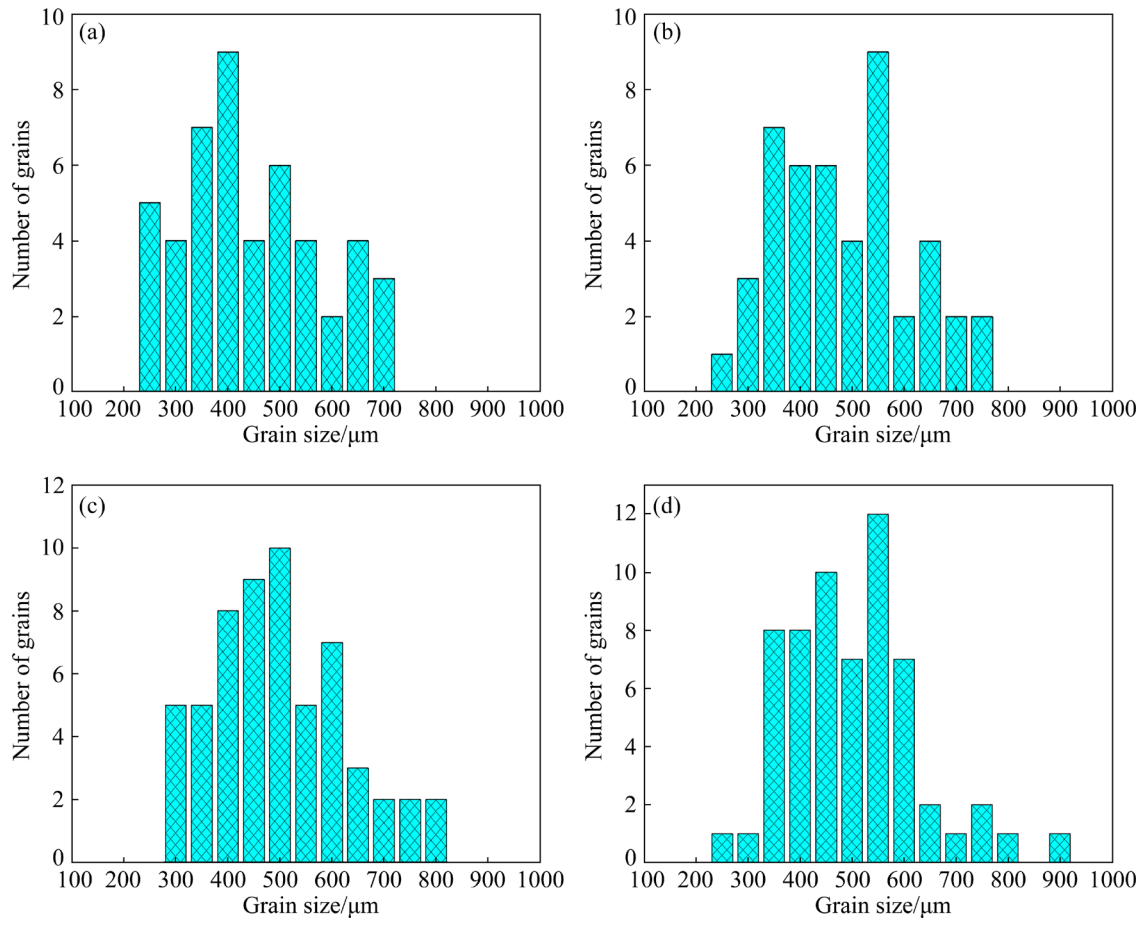


Fig. 7 Grain size distribution in FZ of weld joint obtained under different heat input conditions: (a) 0.232 kJ/mm; (b) 0.265 kJ/mm; (c) 0.312 kJ/mm; (d) 0.406 kJ/mm

distribution in the grain size under all different heat input conditions. The comparison of the plots also revealed the presence of a higher number of larger-sized grains in the FZ at higher heat input state; whereas, under lower heat input conditions, the smaller size grains were more in the count.

Figure 8 shows the variation of average grain size in the FZ and HAZ under different heat input conditions. The average grain size in the FZ was in the range of 460–510 μm; whereas, in the HAZ that was in the range of 100-150 μm. The significant variation in the grain size between FZ and HAZ was attributed to the variation in the thermal cycle experienced by the weld melt pool. During TIG welding, the FZ temperature reached the melting temperature of Ti-6Al-4V alloy; whereas, the HAZ experienced β -transus temperature of the material. Furthermore, the low thermal conductivity of Ti-6Al-4V alloy retained the heat in the weld melt pool for an extended period. Accordingly, slower cooling happened in the melt pool region and yielded relatively coarse grains. In contrast, a

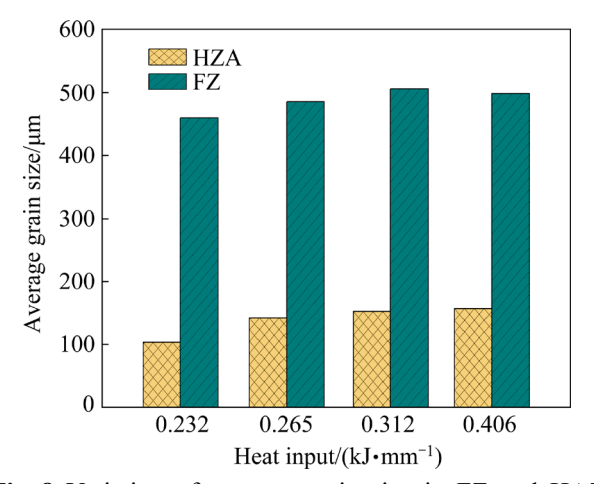


Fig. 8 Variation of average grain size in FZ and HAZ under different heat input conditions

steep temperature gradient as experienced by the HAZ led to the formation of more refined grains.

Figure 8 also indicated a reduction in the average grain size both in FZ and HAZ for the reduced heat input. The average grain size declined from 510 to 460 μ m in the FZ, and from 160 to 100 μ m in the HAZ for the reduction of heat input

from 0.406 to 0.232 kJ/mm. It is expected that due to the induction of a large amount of heat and subsequent melting of a larger volume of the material, the cooling rate of the melt pool declined substantially and consequently yielded larger size grains. However, under lower heat input conditions, a faster cooling experienced by the weld melt pool led to smaller size grains.

3.4 Phase analysis results

of the as-received The XRD patterns Ti-6Al-4V alloy and the FZ of the weld joints under different heat input conditions are depicted in Fig. 9. The patterns show that for the BM, α -Ti peaks are present at 2θ values of 41.17° , 44.93° , 47.13°, 62.58°, 75.07°, 84.62°, and 92.06° corresponding to $(10\bar{1}0)$, (0002), $(10\bar{1}1)$, $(10\bar{1}2)$, $(11\overline{2}0)$, $(10\overline{1}3)$, and $(11\overline{2}2)$ crystallographic planes, respectively; while, β -Ti peak appears at 2θ value of 44.938°, corresponding to $(11\overline{2}0)$ plane. A semi-quantitative analysis performed based on the relative peak intensity of α -Ti and β -Ti phases as represented in Table 2 shows the contents of different phases under different heat input conditions. The data show the presence of 78.14 wt.% α -Ti and 21.86 wt.% of β -Ti phase in the as-received Ti-6Al-4V alloy, which is equivalent to the commercial Ti-6Al-4V alloy. On the contrary, the fraction of the β -Ti phase decreased noticeably in the FZ of the weldment under all different heat input conditions. The values also depicted that the percentage of α -Ti phase increased with the increase of the heat input. The α phase

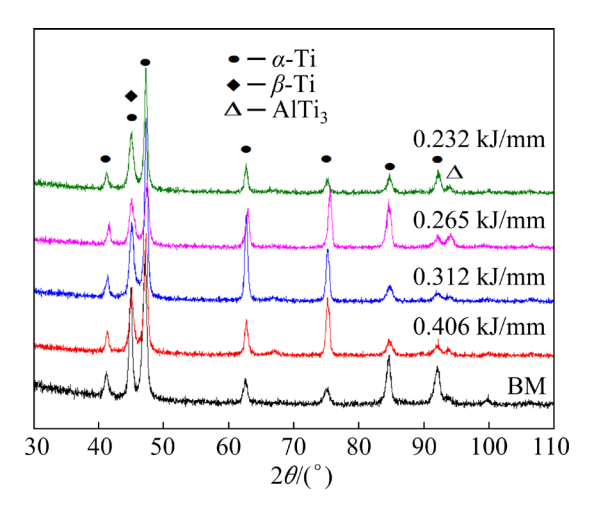


Fig. 9 XRD patterns of TIG-welded surface of Ti-6Al-4V alloy under different heat input conditions along with as-received BM

Table 2 Contents of α and β phases under different welding heat input conditions

Heat input/	Content/wt.%		
$(kJ \cdot min^{-1})$	α phase	β phase	
BM	78.41	21.58	
0.406	84.07	15.93	
0.312	83.91	16.09	
0.265	83.01	16.99	
0.232	81.89	18.11	

enhancement in the FZ is predominantly attributed to partial transformation of β phase to martensitic α phase during the solidification of the weld melt pool. In addition to α -Ti and β -Ti phases, lowintensity AlTi₃ peak was also observed. However, due to the negligible proportion, phases were not considered in the quantitative analysis.

3.5 Microhardness

Microhardness values of the weld joint under different heat input conditions were measured on the lateral section and plotted against the distance from the weld bead centerline as depicted in Fig. 10. Figure 10 exhibited a reasonably higher hardness value in FZ as compared to that of the BM. Depending on heat input, the FZ hardness was recorded between HV_{0.2} 325 to HV_{0.2} 360; whereas, the hardness value in the BM was found $HV_{0.2}300-$ HV_{0.2} 310. The enhanced hardness value in the FZ was predominantly due to the microstructural alteration that occurred during the melting and subsequent solidification of the weld pool [20]. As described in the microstructural analysis, the weld metal is composed of $\alpha+\beta$ phase, martensitic α (needle-type structure), and retaining β with basketweave structure. The formation of martensitic α in the FZ of the Ti-6Al-4V alloy is responsible for the high hardness value [6,21]. The plot indicated that the hardness variation in the FZ at heat inputs of 0.232, 0.265, and 0.312 kJ/mm is from HV_{0.2}325 to HV_{0.2}340. However, at 0.406 kJ/mm heat input, the FZ hardness was stretched up to HV_{0.2} 360, which is sensibly higher as compared to that under lower heat input conditions. As the grain sizes of the FZ marginally increased under higher heat input conditions, it is expected that the formation of significant proportion of α - and martensitic α phases enhanced the hardness value of the weldment. As reported by LIU et al [22] and WAN et al [23], the hardness

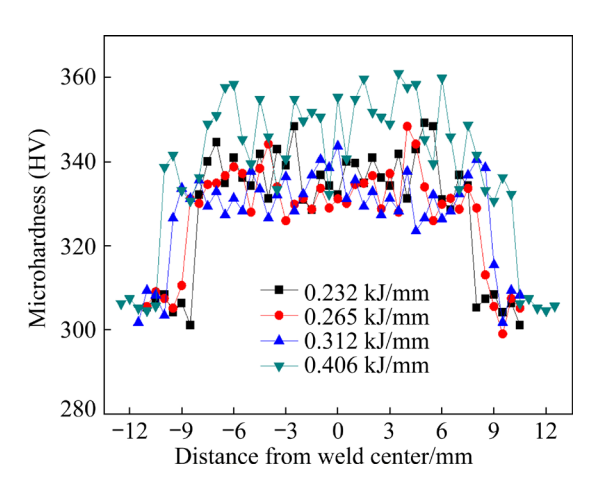


Fig. 10 Variation of microhardness in weld melt pool for weld joint under different heat input conditions

values of α - or α martensitic phases are relatively high as compared to that of the β phase. As evident from the XRD analysis, the proportion of α phase in the FZ increased with the increase of heat input, and consequently, an improved hardness value was recorded. Nevertheless, no significant variation in the hardness value was recorded in the HAZ as compared to that in the FZ. As the HAZ is much narrower as compared to the FZ, and the hardness value was measured at an interval of 0.5 mm, it was

difficult to identify the exact hardness value of the HAZ, and a sharp fall in the hardness value was observed near the HAZ-BM interface.

3.6 Tensile test results

Figure 11(a) illustrates images the post-tensile-test TIG-welded Ti-6Al-4V allov specimens under different heat input conditions. Visual analysis of the specimens showed that under all different heat input conditions, fracture occurred in the FZ only. As discussed in the microstructural analysis, the formation of large amount of α-martensite phase made the FZ more brittle, and the strength of the weldment was also reduced significantly as compared to that of the base material. Henceforth, during tensile test, the failure of the weld joint occurred in the FZ. Similar observation was also reported by WAN et al [23], where the failure of 78 mm-thick TIG-welded Ti-6Al-4V plate happened in the FZ. The load-extension plot and stress-strain plot as recorded during the tensile test for the TIG-welded and the BM specimens are represented in Fig. 11(b, c), respectively. The plot exhibited reasonably lower extension for the weld joints as compared to the BM. The stress-strain plot as

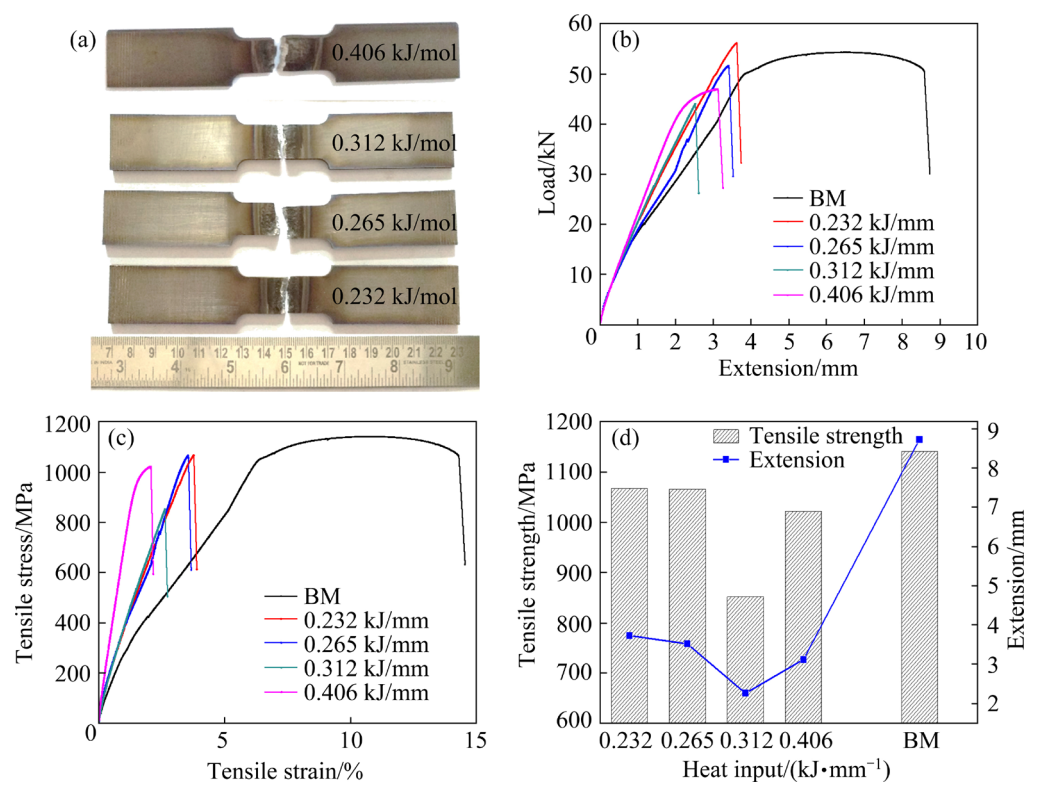


Fig. 11 Weld joint specimens after tensile test (a), load-extension plot (b), stress-strain plot (c), and strength and extension (d) during tensile test of weld joint specimens under different heat input conditions

illustrated in Fig. 11(c) shows that failure of the welded specimen initiated before reaching the ultimate tensile strength (UTS) value of the as-received Ti-6Al-4V alloy, and the stress value plunged suddenly without any plastic deformation. This phenomenon of the stress-strain curve is mainly witnessed in brittle materials. As evident from the microstructure and XRD analysis, the α -martensitic phase in the FZ was reasonably high, which led to strain hardening in the FZ and enhanced the brittleness of the weldment [24].

The tensile strength and the maximum extension of the welded specimens as plotted in Fig. 11(d) indicated that the ultimate tensile strength values of the weld joints produced under different heat inputs (except for 0.312 kJ/mm) are almost equivalent to that of the BM. It was also evident that the tensile strength of the weld joint was reduced marginally with increasing the heat input (except for heat input of 0.312 kJ/mm). For the as-received Ti-6Al-4V alloy, the tensile strength value was recorded as 1140 MPa; whereas, for the weld joints, the tensile strength values changed between 1020 to 1070 MPa (except for the sample with 0.312 kJ/mm heat input, where the value was recorded as 850 MPa). Hence, it may be concluded that the tensile strength values for the TIG-welded Ti-6Al-4V alloy plates are almost equivalent (90%–98%) to those of the BM.

The extensions at failure for the as-received Ti-6Al-4V alloy and the weld joints produced under different heat input conditions (0.232, 0.265, 0.312, and 0.406 kJ/mm) were recorded as 8.73, 3.73, 3.52, 2.26 and 3.12 mm, respectively. Similarly, the percentage of elongations were found to be 14.0%, 3.9%, 3.7%, 2.4%, and 3.3%, respectively. These data revealed a steep reduction in the ductility of the weld joints as compared to the BM. The percentages of elongations of the welded specimens under different heat input conditions are significantly lower compared to that of the BM due to the post welding microstructure alteration. As discussed in the microstructure analysis, the weld zone consists of acicular- α , martensitic α phases and Widmanstätten α colony separated by prior β boundaries. Martensitic α is a hard and brittle phase, which reduced the ductility of the material. Accordingly, the percentage of elongations of the welded specimens was reduced significantly. However, the data also indicated that with the increase in heat input, the extension of the weldment during failure was reduced gradually. Hence, it can be concluded that the ductility of the weld joint was improved for the reduction of heat input employed during the TIG welding of Ti-6Al-4V alloy. The extension of the test specimen during the tensile test largely depends on the weld joint microstructure. Owing to the formation of a martensitic structure, the ductility of the weld joint was reduced drastically, which resulted in lower extensions of the welded specimens as compared to the BM. KUMAR and SHAHI [10] showed that lower heat input during the TIG welding of AISI 304 steel produced fine grain microstructure and consequently enhanced the ductility of the weld joint. In the present case, lower grain size was also observed in the weldment for reducing the heat input.

3.7 Fractograph of tensile test specimen

To comprehend the fracture mechanism and mechanical properties of the weld joint, the fractured surfaces of the tensile test specimens were examined through optical and scanning electron microscopy. Figure 12 illustrates the OM images of the fractured surfaces for as-received Ti-6Al-4V alloy and the weld joints with the heat inputs of 0.232 and 0.406 kJ/mm, respectively. Here, maximum and minimum heat input conditions were considered to analyze the effect of heat input more accurately. From the images, necking was observed for the as-received Ti-6Al-4V alloy, which is the characteristic of a ductile material. However, no specific necking was witnessed for the weld joints. The formation of martensite structure in the weldment and consequent reduction in the ductility of the weld joint led to the failure of the weld specimen without appreciable necking.

From the SEM images as depicted in Fig. 13, an appreciable difference in the fractured morphology can be observed for the as-received Ti–6Al–4V alloy and the weld specimens. The images (Figs. 13(a, b)) revealed that the fractured surface of the as-received BM was of dimpleshaped feature in combination with a homogeneous flat faceted structure and river line pattern. Due to the ductile nature of the BM, the specimen got elongated and experienced plastic deformation before the failure. As suggested by YANG et al [25], these features are primarily obtained owing to the

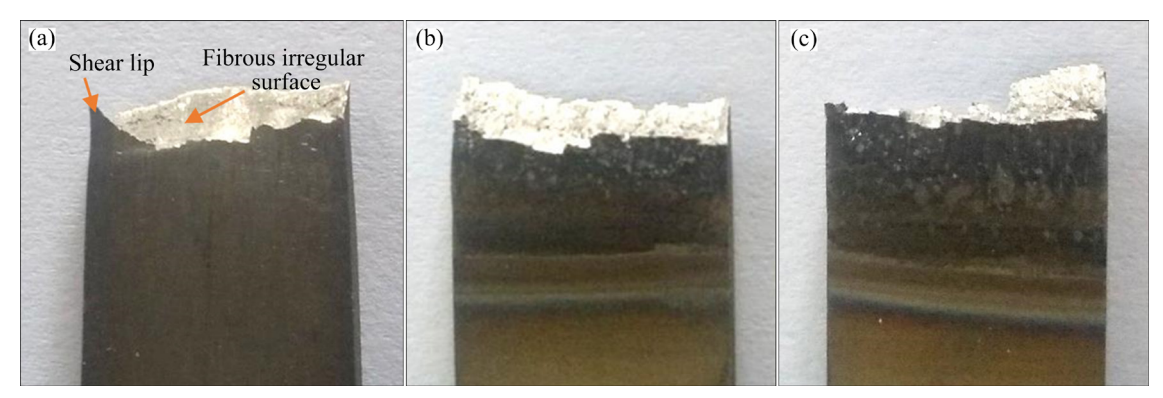


Fig. 12 OM images showing fractured surfaces of tensile specimens: (a) BM; (b, c) Weld joints with heat inputs of 0.232 kJ/mm and 0.406 kJ/mm, respectively

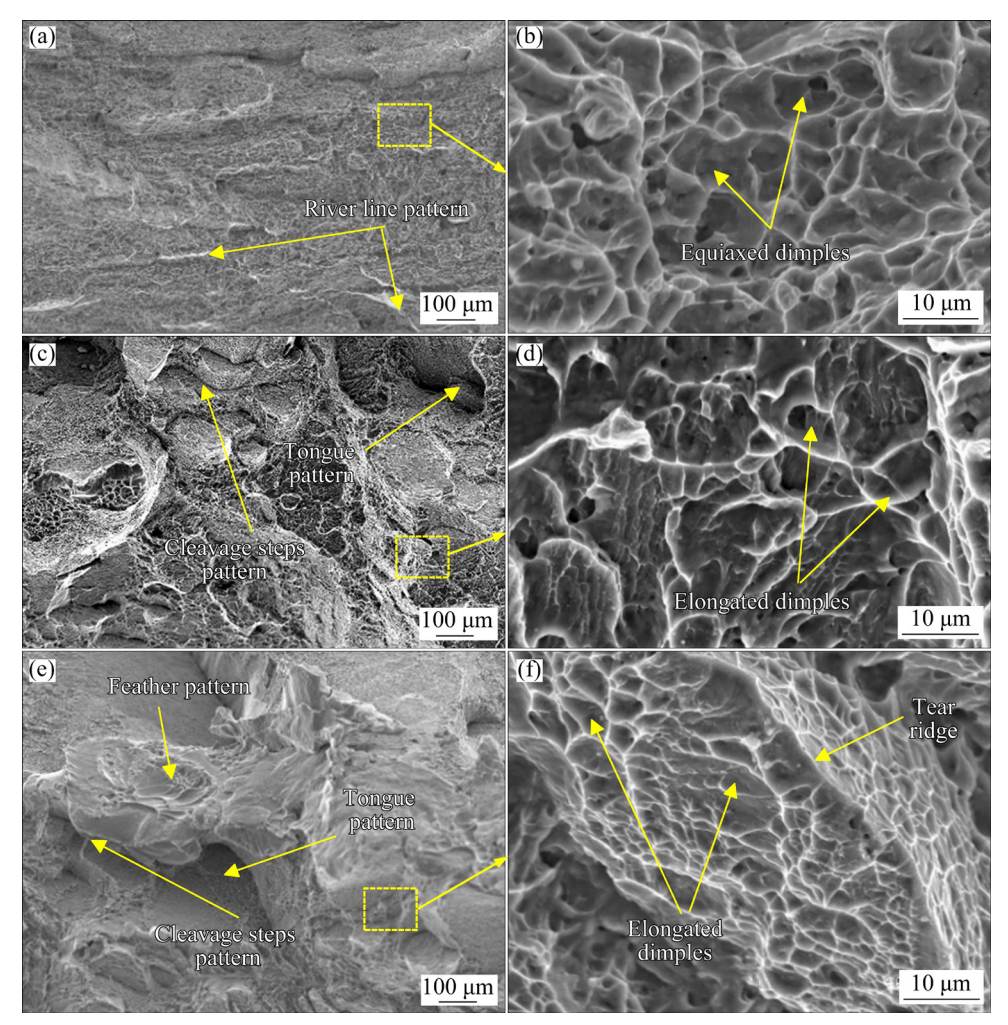


Fig. 13 SEM images showing fractured morphologies of tensile specimens: (a, b) BM; (c, d) Weld joint at heat input of 0.232 kJ/mm; (e, f) Weld joint with heat input of 0.406 kJ/mm

ductile failure of the material. On the contrary, the images (Figs. 13(c) and (e)) of the fractured surface of the weld joint showed the presence of cleavage steps, tongue, and feather-like patterns at the failure location. These cleavage steps, tongue, and feather-like patterns were predominantly obtained during the brittle failure of the weld joint. The magnified

images of the fractured surfaces of the weld joints, as illustrated in Figs. 13(d) and (f), also showed the formation of dimple patterns, which were elongated in shape with cleavage facets. The fractured surface of the weld joint at higher heat input (0.406 kJ/mm) exhibited larger population of non-uniform elongated dimples along with tear ridges on its

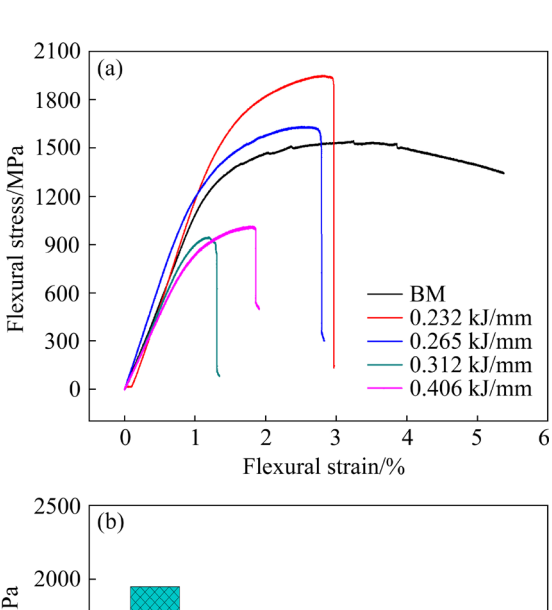
surface. However, elongated dimples are nearly uniform, and tear ridges are almost absent on the fractured surface of the weld joint for lower heat input (0.232 kJ/mm). The material strength and ductility largely depended on the size and shape of the dimples that appeared on the fractured surface during the tensile test [26]. The uniform and smaller size dimples were characteristic of high strength and ductile materials. Hence, non-uniform and elongated or parabolic-shaped dimples on the fractured surface of the welded specimen with higher heat input suggested lower ductility than the weld joint obtained at lower heat input. According to CAO and JAHAZI [6], the cleavage pattern on the fractured surface mostly appeared due to the reduction in ductility of the weld joint. The above observations indicated a mixed-mode of failure (both ductile and brittle fracture) in the weld joint during the tensile test, and the ductility of the weld joint was reduced with the increase of heat input during the welding process.

3.8 Bend test results

After the bend test, the bend angles of the test specimens were measured using a protractor, and values were correlated with the heat input employed during the welding process. The results indicated that for the as-received BM, the recorded bend angle was approximately 48°; whereas for the welded specimens, lower bend angles, i.e. in the range of 21°-36°, were noted. For the specimens with the heat inputs of 0.232, 0.265, 0.312, and 0.406 kJ/mm, the bend angles were recorded as 36°, 32°, 21°, and 29°, respectively. The data indicated that with the increase of heat input, the bend angle was reduced almost gradually (except for the specimen with 0.312 kJ/mm of heat input). A higher bend angle signifies the formability of the material. Hence, the analysis revealed superior formability of the welded specimens for the lower heat input employed during the welding process. During laser welding of Ti-6Al-4V alloy, LISIECKI [8] showed that the bend angle increased from 18° to 37° with reducing the heat input from 96 to 60 J/mm, and the brittleness of the weld joint augmented with the increase in heat input.

Flexural strength is the capacity of a material to resist deformation under bending or the maximum bending stress withstood by the material before yielding. It is also referred to as the bending

strength of the material. The flexural stress-strain curves and the flexural strength values for the welded samples under different heat input conditions and the BM are recorded during the bend test, as illustrated in Fig. 14. Figure 14(a) showed that the flexural stress of the weld joint under the lower heat input condition was higher than that of the BM, and the value was reduced with the increase of heat input. The magnitude of flexural strength, as illustrated in Fig. 14(b), showed that the strengths of the weld joints with lower heat input (0.232 and 0.265 kJ/mm) were 1950 and 1630 MPa, which were approximately 27% and 6% higher than that of the as-received BM. However, the flexural strengths for the weld joint with higher heat inputs (0.312 and 0.406 kJ/mm) were recorded as 945 and 1015 MPa, approximately 39% and 35% lower than that of the BM, respectively. It can also be noted that the maximum flexural strain of the BM was approximately 5.5%. However, the flexural strain values for the weld joints at the heat inputs of 0.232, 0.265, 0.312, and 0.406 kJ/mm were



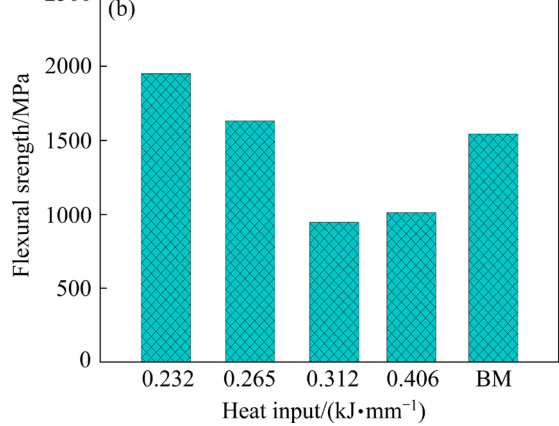


Fig. 14 Flexural stress-strain curves (a) and flexural strength (b) of BM and weld joints under different heat inputs

approximately 3%, 2.5%, 1.2%, and 1.8%, respectively, much lower than that of the BM. The plot also showed an increasing trend in the flexural strain values for reducing heat input (except for the weld joint at 0.312 kJ/mm). GAO et al [27] reported that the formation of residual β phase became more prominent during electron beam welding for employing lower heat input, which consequently exhibited higher ductility in the weldment as compared to the higher heat input condition. In the present case, it was expected that at lower heat input (combination of higher current and higher scan speed), due to the smaller size grain formation, the strength of the weld joint was improved substantially. On the other side, at higher heat input, the formation of larger size grains reduced the weld joint strength considerably. Furthermore, under higher heat input condition, the formation of larger percentage of α phase enhanced the brittleness of the weldment. Thus, the flexural strength of the weld joint increased for reducing the heat input during the TIG welding of Ti-6Al-4V alloy.

4 Conclusions

- (1) The full penetration weld joint of 3 mm-thick Ti-6Al-4V alloy plate was obtained at 150 A current and 2.3 mm/s scan speed, which corresponded to heat input of 0.406 kJ/mm. By reducing the heat input (from 0.406 to 0.232 kJ/mm), with increasing the welding current and scan speed simultaneously, full penetration welding with superior mechanical properties was achieved.
- (2) The microstructural analysis revealed that the HAZ was composed of primary- α , primary- β , and acicular- α phases while the FZ was characterized by larger size grains consisting of Widmanstätten α colony separated by prior β boundaries. The average grain size both in FZ and HAZ was reduced with the reduction of heat input during the welding process.
- (3) The tensile strength of the full penetrated weld joint increased almost gradually with the reduction of heat input. The maximum tensile strength was achieved under the lowest heat input (0.232 kJ/mm) condition, which was 98% of the BM strength. Post tensile test fracture surface analysis revealed a mixed-mode of failure (ductile and brittle fracture) in the weld joint. Due to the

lower ductility of the weld joint under higher heat input conditions, non-uniform elongated dimple formation was witnessed.

(4) Compared to that of the BM, the flexural strength of the weld joint was enhanced by up to 27% under lower heat input condition (0.232 kJ/mm). However, at higher heat inputs (0.312 and 0.406 kJ/mm), the flexural strength was reduced by almost 39% and 35%, respectively as compared to that of the BM.

References

- [1] VAHIDSHAD Y, KHODABAKHSHI A H. An investigation of different parameters on the penetration depth and welding width of Ti-6Al-4V alloy by plasma arc welding [J]. Welding in the World, 2021, 65: 485-497.
- [2] LI Jun-ping, SHEN Yi-fu, HOU Wen-tao, QI Yi-ming. Friction stir welding of Ti-6Al-4V alloy: Friction tool, microstructure, and mechanical properties [J]. Journal of Manufacturing Processes, 2020, 58: 344-354.
- [3] AKMAN E, DEMIR A, CANEL T, SINMAZÇELIK T. Laser welding of Ti₆Al₄V titanium alloys [J]. Journal of Materials Processing Technology, 2009, 209: 3705–3713.
- [4] WANG Shao-gang, WU Xin-qiang. Investigation on the microstructure and mechanical properties of Ti-6Al-4V alloy joints with electron beam welding [J]. Materials & Design, 2012, 36: 663-670.
- [5] PANDEY C, MAHAPATRA M M, KUMAR P, SAINI N. Comparative study of autogenous tungsten inert gas welding and tungsten arc welding with filler wire for dissimilar P91 and P92 steel weld joint [J]. Materials Science and Engineering A, 2018, 712: 720-737.
- [6] CAO X, JAHAZI M. Effect of welding speed on butt joint quality of Ti-6Al-4V alloy welded using a high-power Nd:YAG laser [J]. Optics and Lasers in Engineering, 2009, 47: 1231-1241.
- [7] LEYENS C, PETERS M. Titanium and titanium alloys: Fundamentals and applications [M]. New York: Wiley-VCH, 2003.
- [8] LISIECKI A. Welding of titanium alloy by disk laser [C]// Proc. SPIE. Washington: Society of Photo-optical Instrumentation Engineers, 2012: 1–12.
- [9] KARPAGARAJ A, SHANMUGAM N S, SANKARANA-RAYANASAMY K. Some studies on mechanical properties and microstructural characterization of automated TIG welding of thin commercially pure titanium sheets [J]. Materials Science and Engineering A, 2015, 640: 180–189.
- [10] KUMAR S, SHAHI A S. Effect of heat input on the microstructure and mechanical properties of gas tungsten arc welded AISI 304 stainless steel joints [J]. Materials & Design, 2011, 32: 3617–3623.
- [11] MERAN C. Prediction of the optimized welding parameters for the joined brass plates using genetic algorithm [J]. Materials & Design, 2006, 27: 356–363.
- [12] LIU Zu-ming, FANG Yue-xiao, CUI Shuang-lin, LUO Zhen,

- LIU Wei-dong, LIU Zhi-yi, JIANG Qu, YI Song. Stable keyhole welding process with K-TIG [J]. Journal of Materials Processing Technology, 2016, 238: 65–72.
- [13] LAKSHMINARAYANAN A K, BALASUBRAMANIAN V, ELANGOVAN K. Effect of welding processes on tensile properties of AA6061 aluminium alloy joints [J]. The International Journal of Advanced Manufacturing Technology, 2009, 40: 286–296.
- [14] BOCCARUSSO L, ARLEO G, ASTARITA A, BERNARDO F, FAZIO P D, DURANTE M, MINUTOLO F M C, SEPE R, SQUILLACE A. A new approach to study the influence of the weld bead morphology on the fatigue behaviour of Ti-6Al-4V laser beam-welded butt joints [J]. The International Journal of Advanced Manufacturing Technology, 2017, 88: 75-88.
- [15] MRIDHA S, BAKER T N. Overlapping tracks processed by TIG melting TiC preplaced powder on low alloy steel surfaces [J]. Materials Science and Technology, 2015, 31: 337–343.
- [16] RASOOL G, MRIDHA S, STACK M M. Mapping wear mechanisms of TiC/Ti composite coatings [J]. Wear, 2015, 328/329: 498–508.
- [17] KABIR A S H, CAO X J, GHOLIPOUR J, WANJARA P, CUDDY J, BIRUR A, MEDRAJ M. Effect of postweld heat treatment on microstructure, hardness, and tensile properties of laser-welded Ti-6Al-4V[J]. Metallurgical and Materials Transactions A, 2012, 43: 4171-4184.
- [18] BABU N K, RAMAN S G S, MYTHILI R, SAROJA S. Correlation of microstructure with mechanical properties of TIG weldments of Ti-6Al-4V made with and without current pulsing [J]. Materials Characterization, 2007, 58: 581-587.
- [19] DING R, GUO Z X, WILSON A. Microstructural evolution of a Ti-6Al-4V alloy during thermomechanical processing [J]. Materials Science and Engineering A, 2002, 327: 233-245.

- [20] CHOI J W, AOKI Y, USHIODA K, FUJII H. Linear friction welding of Ti–6Al–4V alloy fabricated below β-phase transformation temperature [J]. Scripta Materialia, 2021, 191: 12–16.
- [21] MENDEZ P F, EAGAR T. Penetration and defect formation in high-current arc welding [J]. Welding Journal, 2003, 82: 296–306.
- [22] LIU H, NAKATA K, YAMAMOTO N, LIAO J. Microstructural characteristics and mechanical properties in laser beam welds of Ti₆Al₄V alloy [J]. Journal of Materials Science, 2012, 47: 1460–1470.
- [23] WAN L, HUANG Y, LV S, HUANG T, LI C, FENG J. Narrow-gap tungsten inert gas welding of 78-mm-thick Ti-6Al-4V alloy [J]. Materials Science and Technology, 2016, 32: 1545-1552.
- [24] KRAUSS G, MATLOCK D K. Effects of strain hardening and fine structure on strength and toughness of tempered martensite in carbon steels [J]. Journal De Physique IV, Proceedings, EDP Sciences, 1995, 5(C8): 51–60.
- [25] YANG Zhou, QI Bo-jin, CONG Bao-qiang, LIU Fang-jun, YANG Ming-xuan. Microstructure, tensile properties of Ti-6Al-4V by ultra-high pulse frequency GTAW with low duty cycle [J]. Journal of Materials Processing Technology, 2015, 216: 37-47.
- [26] MAGUDEESWARAN G, BALASUBRAMANIAN V, BALASUBRAMANIAN T S, REDDY G M. Effect of welding consumables on tensile and impact properties of shielded metal arc welded high strength, quenched and tempered steel joints [J]. Science and Technology of Welding and Joining, 2008, 13(2): 97–105.
- [27] GAO Fu-yang, GAO Qi, JIANG Peng, LIU Zhi-ying, LIAO Zhi-qian. Microstructure and mechanical properties of Ti6321 alloy welded joint by EBW [J]. International Journal of Lightweight Materials and Manufacture, 2018, 1: 265–269.

减少热输入对 TIG 自熔焊 Ti-6Al-4V 合金的影响

Kamlesh KUMAR, Manoj MASANTA

Department of Mechanical Engineering, National Institute of Technology Rourkela, Rourkela 769008, India

摘 要:采用带有气体保护装置的 TIG 自熔焊技术以对接接头结构形式焊接厚度为 3 mm 的 Ti-6Al-4V 合金板。在适当热输入条件下获得完全熔透的焊接接头后,结合较高焊接电流和扫描速度以减少热输入开展后续实验。对不同热输入条件下获得的焊接接头进行深入的显微组织分析。结果表明,显微硬度、拉伸强度和断裂强度之间存在强相关性。采用较低的热输入可以显著提高焊接接头的力学性能。这是由于在较低热输入条件下,热输入的变化导致初生 α 相、初生 β 相和马氏体 α 相发生改变,从而改善了焊接接头的力学性能。随着热输入从 0.406 kJ/mm降低到 0.232 kJ/mm,焊接接头的拉伸强度和断裂强度分别从 1020 和 1015 MPa 增加到 1070 和 1950 MPa。在最小热输入(0.232 kJ/mm)的情况下,接头的拉伸强度达到基材的 98%。实验结果证明在低热输入条件下 TIG 焊焊接 Ti-6Al-4V 合金的潜力。

关键词: TIG 焊; Ti-6Al-4V 合金; 热输入; 拉伸强度; 显微组织